Experimental study of two kinds of hard marine growth effects on the hydrodynamic behavior of a cylinder submitted to wave and current loading

Antoine Marty, Franck Schoefs, Guillaume Damblans, Jean-Valery Facq, Benoît Gaurier, Gregory Germain

Experimental study of two kinds of hard marine growth effects on the hydrodynamic behavior of a cylinder submitted to wave and current loading.

A. Marty[a], F. Schoefs[b], G. Damblans[c], J-V. Facq[a], B. Gaurier[a], G. Germain[a]

[a]*Ifremer, Marine Structure Laboratory, 150 Quai Gambetta 62200 Boulogne sur Mer, France*
[b]*GeM, UMR CNRS 6183, Université de Nantes, 2 rue de la Houssinière, 44322 Nantes, France*
[c]*France Energies Marines, 525 Avenue Alexis de Rochon, 29280 Brest, France*

Abstract

The presence of marine growth increases submarine structures diameter and roughness and thus the hydrodynamic loading due to wave and current excitation. In this paper, two kinds of hard roughness (mussels and corals) are studied experimentally. In order to cover a wide range of the dimensionless numbers (Reynolds number, Keulegan-Carpenter number and reduced speed), three kind of trials are carried out: current only, forced motions and a combination of forced motions and current. Two equivalent diameters are used for the calculation of the hydrodynamic coefficients: an equivalent diameter corresponding to the closed volume of the system, where no fluid is permitted, and an equivalent diameter based on the projected area of the colonized structure for the drag coefficient, and on the total volume for inertia coefficients.
Results show that these coefficients are up to 4 times higher than those obtained for a reference cylinder. The use of a different specific diameter for inertia and drag coefficient leads to fit all results with the reference cylinder results. This standardization prove that the knowledge of the volume and the projected surface of the cylindrical structure could simplify the forces estimation applied on the system just by knowing the corresponding smooth one.

Keywords: Cable, Marine growth, Roughness, Drag coefficient, Coral, Mussel

1. Introduction

Offshore structures such as jacket-platform, risers or submarine cables are subject to biofouling and marine growth colonization which can have a strong impact on the hydrodynamic behavior of the structure. These unwanted organisms lead to an increase of the size and the mass of the structure and this affects drag and inertia phenomena under wave and current conditions, especially when those marine growth have large and hard sizes. The presence of roughness on cylinders has been widely investigated in the literature by Achenbach and Heinecke [1], Schlichting [19], Sarpkaya [16], [18], [17], Jusoh and Wolfram [10] or Xiaojie et al. [28] and Vanhinsberg [26] more recently. These studies agree with the statement that the roughness tends to highly modify the flow around the structure and decrease the critical Reynolds number where the transition between laminar and turbulent occurs, but they all focus on a relatively low roughness parameter (lower than 0.02) defined by the ratio k/D where k characterizes the roughness height and D the characteristic length of the structure, here the equivalent diameter. The few studies which investigated large roughness highlight that the critical transition does not occur in the flow velocity range studied for the rough cases. Moreover, they showed that the

hydrodynamic behavior is quite different. Indeed, Teng and Nath [23] and Marty et al. [12] showed that for large roughness, the drag and inertia coefficients can be from 1.5 to 4 times higher than those obtained for a smooth cylinder in the same conditions of wave and current but they did not observe any dependence of the relative roughness on the inertia coefficient values for the studied conditions. In the roughness range studied (from $k/D = 0.06$ to 0.13), inertia behavior is not impacted by the presence of roughness and the resulting mass increase, contrary to the drag phenomena which are amplified with the increase of the roughness. That leads to the conclusion that the increased diameter by the marine growth thickness seems to be a preponderant factor in the overall evolution of coefficients compared to the mass and the added mass increase of the structure. A comparison between the calculated results and standards (API [3] and DNV [6] for example) is made and show that the standard predictions of the drag coefficient are quite good for trials under current as long as they stay in the sub-critical regime. This is not the case for tests under wave and current conditions where calculated results are different from predictions by a factor 2 for the oscillating drag coefficient and 1.5 for the inertia coefficient. This confirms that the most influencing parameter of a hard fouling cover is the surface protuberance field seen as a roughness by the flow which can not be ignored.

Moreover, Theophanatos [24] or [25], who investigated hydrodynamic loading on macro-roughened cylinders of various aspect ratios showed that the roughness parameter can not be the only factor to take into account for characterize the complexity of the fluid structure interaction. Indeed, the type of roughness (hard or smooth), the areal density (percentage of presence on the structure) and the shape of the roughness have also to be taken into account. Marty et al. [11] who investigated the effect of large and real shaped roughness on the hydrodynamic behavior of a submarine cable under wave and current conditions confirmed this point about shape importance. Moreover they compared uniformly distributed roughness with non-uniformly distributed roughness and also showed that this point had a real impact on the hydrodynamic behavior of the cable. According to Theophanatos's work, the type of surface roughness, and particularly if it is a hard or smooth roughness, have a considerable impact on the hydrodynamic behavior. In Henry et al. [9] they compared hard marine growth (sand roughness) with soft marine growth (artificial fur) and showed significant differences between these two types of biofouling, on the vortex shedding behavior such as the mechanical behavior. Zeinoddini et al. [29] proposed a comparative study on vortex induced vibrations generated by several types of roughness including hard and soft, and full or partial coverage. The experimental results showed that the fouling played an important roles in the overall wake dynamics and the cylinder response.

Finally, the density of the marine growth and its shape seems to be preponderant element in calculating hydrodynamic coefficients such as inertia and drag coefficients. That is why it is so important to constitute experimental database with different kind of roughness, especially for large scale roughness which have not yet received due attention in the literature. Therefore, this work focuses on the experimental study of two kinds of hard marine growth under wave and current conditions. The first one is representative to a mussel colonization uniformly or non-uniformly distributed along the cylinder, as encountered in temperate zone (see figure 1 and Repecaud et al. [15]). The second one is representative to a coral colonization that means very large and dense, as encountered in tropical zone (see figure 2). The mussel roughness already presented in [11] include seven configuration $0 < k/D < 0.14$. The coral roughness includes two configurations with very large

macro-roughened cylinders whose roughness height is 80 *mm* compared with the 200 *mm* cylinder on which it is fixed. The difference between the two corals configurations is the addition on one of them of "micro" roughness (3 *mm*) which is very small compared to the preponderant part of the roughness. The roughness parameter k/D of this coral set-up reaches 0.4. To our knowledge, no similar study exists with such a large scale roughness. Tests were conducted in a flume tank under current conditions first, then horizontal imposed motions condition to be representative of the waves orbital velocity, and finally the combination of both conditions. A wide range of classical normalized numbers such as the Reynolds number (R_e), the Keulegan-Carpenter number (KC) and the reduced speed (U_r) were studied in order to be as close as possible to the sea conditions. These tests are carried-out at full-scale, removing the Reynolds similitude issue. The purpose of the tests is firstly to quantify the impact of large roughness on the cylinder response about drag and inertia phenomena by comparing them with a smooth cylinder under the same loading. Thereafter, the use of a specific and different equivalent diameter for the calculation of the inertia coefficients and the drag coefficients is discussed.

Figure 1: Illustration of mussel colonisation on a mooring line (West coast of France on a 0.1m diameter mooring line at 10m depth) [15].

In this paper, we first describe the experimental set-up including the experimental process to simulate large fouling (corals) concretions on a cable and the calculation method of hydrodynamic coefficients. Then, we will present the results of the experimental campaigns. The mean drag coefficient (C_D) for trials under current and both inertia (C_m) and drag coefficients (mean one C_D and oscillating one C_d) for trials under combined current and forced motions will be compared for all configurations. Finally, the choice of the equivalent diameter used in the calculation of the hydrodynamic coefficients which is a key-point of this kind of study is discussed. First, the coefficients are calculated using the equivalent diameter corresponding to the closed volume where no fluid is permitted. In a second time, the coefficients are calculated using a specific equivalent diameter for drag coefficient, based on the projected area of the system, and a specific one for inertia coefficients, based on the total volume of the system.

Figure 2: Illustration of corals colonisation on a jacket of marine platform in West Africa, with a tubular bracing structure of 0.2 to 2m diameter.

2. Experimental set-up

The assembly is based on the use of a 6 degrees of freedom (DOF) hexapod to simulate wave effects on an instrumented cylinder (rough and smooth) submitted to a current. In this section, the assembly, the roughness model and the test cases are presented.

2.1. Assembly and instrumentation

The tests are carried out in the wave and current circulating tank of Ifremer, located in Boulogne-sur-Mer (France) and presented in Fig.3. The test section is: $18m$ long $\times$ $4m$ wide (w_t) $\times$ $2m$ high (h_t). In this work, the three instantaneous velocity components are denoted (U, V, W) along the (X, Y, Z) directions respectively (Fig.3 and Fig.4). Each instantaneous velocity component is separated into a mean value and a fluctuating part according to the Reynolds decomposition: $U = \overline{U} + u'$, where an overbar indicates the time average. The incoming flow ($\overline{U_\infty}$, $\overline{V_\infty}$, $\overline{W_\infty}$) is assumed to be steady and constant. By means of a grid and a honeycomb (that acts as a flow straightener) placed at the inlet of the working section, a turbulent intensity of $I = 1.5\%$ is achieved, see Gaurier et al. [7].

An overview of the global set-up is presented on figure 4 . The cylinder movements are generated using a 6-DOF hexapod on which the structure and the instrumentation are fixed.

As shown on figure 4, the cylinder is horizontally mounted so that the cylinder is located in the middle of the test section (at one meter depth). The 2 m length cylinder is perpendicular to the direction of the upstream flow. To simulate wave conditions, the hexapode moves with an oscillating and periodic motion in parallel to the flow to represent the horizontal part of the waves orbital velocity. The hexapod motions along the Ox axis are characterized by its amplitude (A_x) and its frequency (f). The axis coordinate system (X, Y, Z, in red on the Fig.4) is chosen so that the Ox axis is in the same direction as the current. The Oy axis is across the width of the basin and the Oz axis is vertical and oriented downward.

Two 6 components load cells, fixed at each extremity of the cylinder enable the forces applied to the cylinder to be measured. The location of these load cells is identified by their own axis systems as shown on Figure 4.

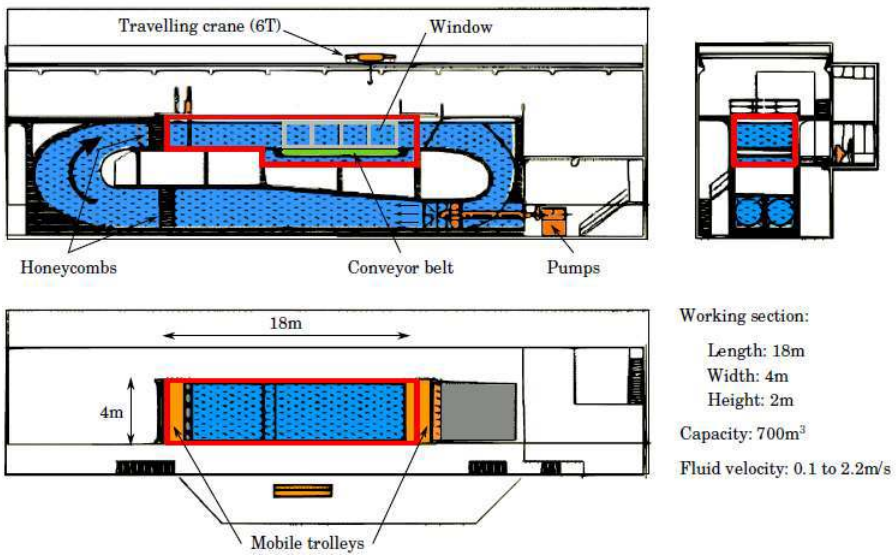

Figure 3: IFREMER Flume tank in Boulogne-sur-Mer.

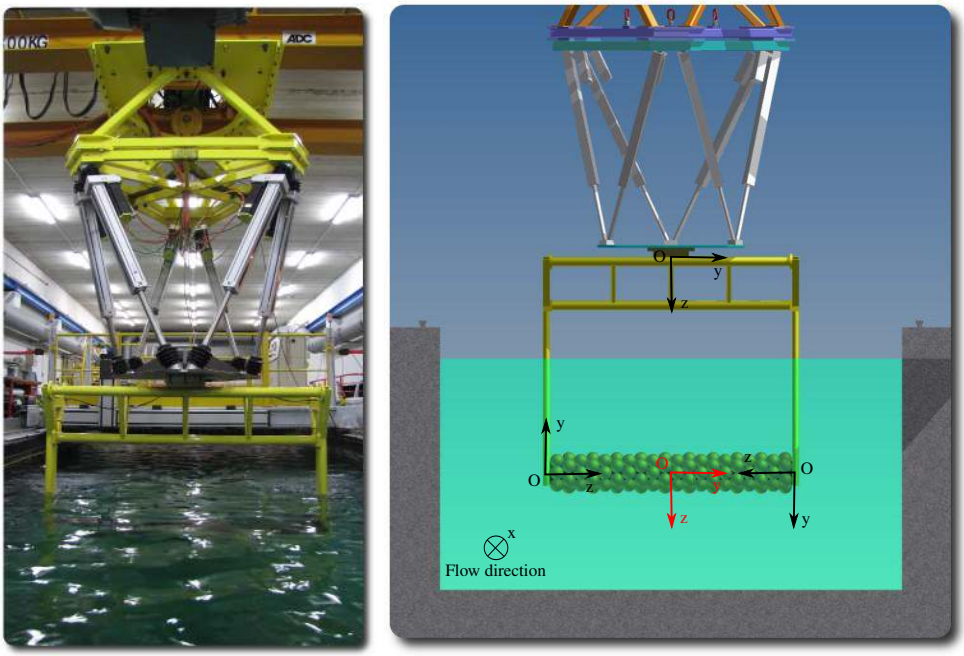

Figure 4: Presentation of the global set-up with the 6-DOF hexapod (left), the macro-roughened cylinder (right).

The two cylindrical load cells measure the forces applied on the cylinder only, half of the total load for each cell with load cells range of $F_{x,y,z} = \pm 1500\ N$ (accuracy of 0.75 N). The cylinder is free to rotate around the z axis without any constraints along the x axis in order to build a non-hyperstatic assembly. With this experimental set-up, the degree of confidence in the results is estimated at 95% knowing that the uncertainty budget is lower than 5% and the repeatability/reproductibility of the measurements is good (the precision of the hexapod is under 0.5 mm, the upstream flow turbulence intensity is 1.5% and the blockage ratio is, for the highest cylinder external diameter, lower than 10%).

2.2. Test cases

The purpose of this work is to experimentally study two kinds of hard marine growth, mussels and corals, under wave and current conditions. Six mussel configurations called $C1$, $C2$, $C1/S$, $C2/S$, $C1/C2$, $C2/C1$ (see figure 5) and two macro-roughened configurations representative to coral colonization called $C3$ and $C4$ (see figures 6 and 7) lead to height roughened configurations with a roughness parameter going from smooth to 0.4. A smooth configuration called S is also used as a reference case. This would provide a large database of results for cylinder with large roughness under wave and current excitation.

The mussel configurations, which reproduce the roughness with a highly realistic representation of mussel colonization through 3D printing covers, have been presented in details in Marty et al. [11] and Figure 5 reminds the overall shape. The coral configurations, represented on figure 6, is representative to corals commonly encountered on marine platforms located in tropical zone (West Africa, Fig. 2).

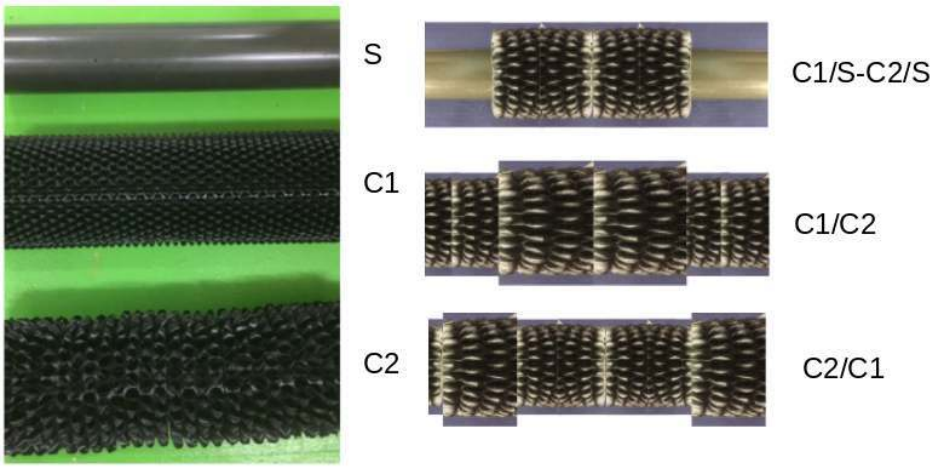

Figure 5: Representation of the seven tested configurations presented in Marty et al. [11]

To this aim, small scale roughness have been estimated directly by measurements on the samples collected in situ in the Gulf of Guinea at two different depths (6 meters and 17 m eters). In Boukinda et al. [5], the main trends of the colonization typology and process in Gulf of Guinea, where corals prevail on the surface of the structural elements, are given. The coral modelization used in this study is based on the predictive models of marine growth development and their statistical parameters proposed in Boukinda et al. [5] and Schoefs and Tran [20]. The main assumption concern the representation of the coral surface roughness: when the polyps are retracted, sharp edges can be encountered while when the animals out feeding, the surface is smooth. From these models, it was deduced that the small-scale roughness (micro-roughness) was 3 mm depths and 15 mm of diameter. It was physically simulated by creating small craters equally distributed with the centres of the craters placed every 20 mm (see Figure 7). The range of large-scale roughness was assessed from a set of pictures as shown in Figure 2. They are based on spheres of diameter 120 mm uniformly distributed around and along the cylinder as shown on figures 6 and 8 . Therefore, the configuration called $C3$ corresponds to the cylinder on which is fixed the large-scale coral roughness and the $C4$ roughness configuration corresponds to the same large-scale roughness as $C3$ on which the small craters were added to realize a small roughness in addition of the large-scale one. The details and the dimensions of both coral roughness ($C3$ and $C4$) are given in Figure 7.

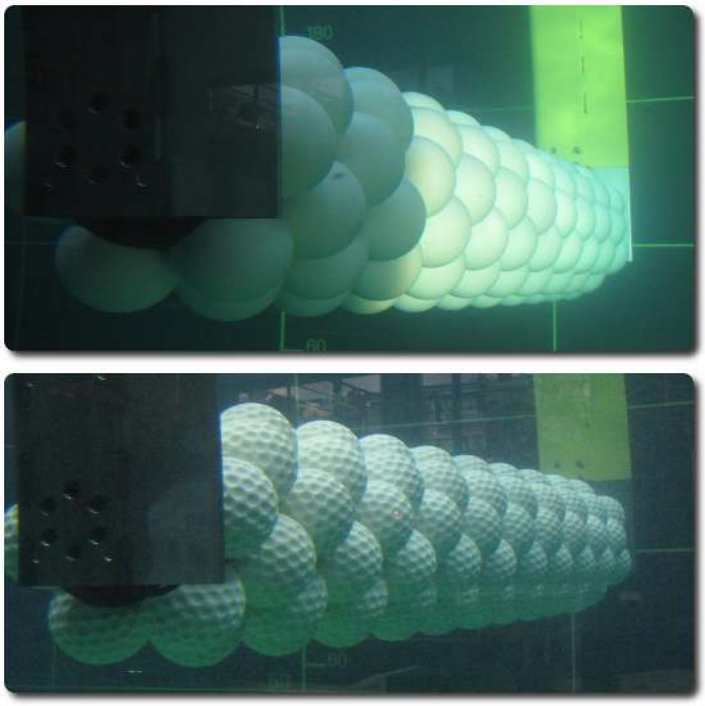

Figure 6: Representation of the large-scale coral roughness configurations

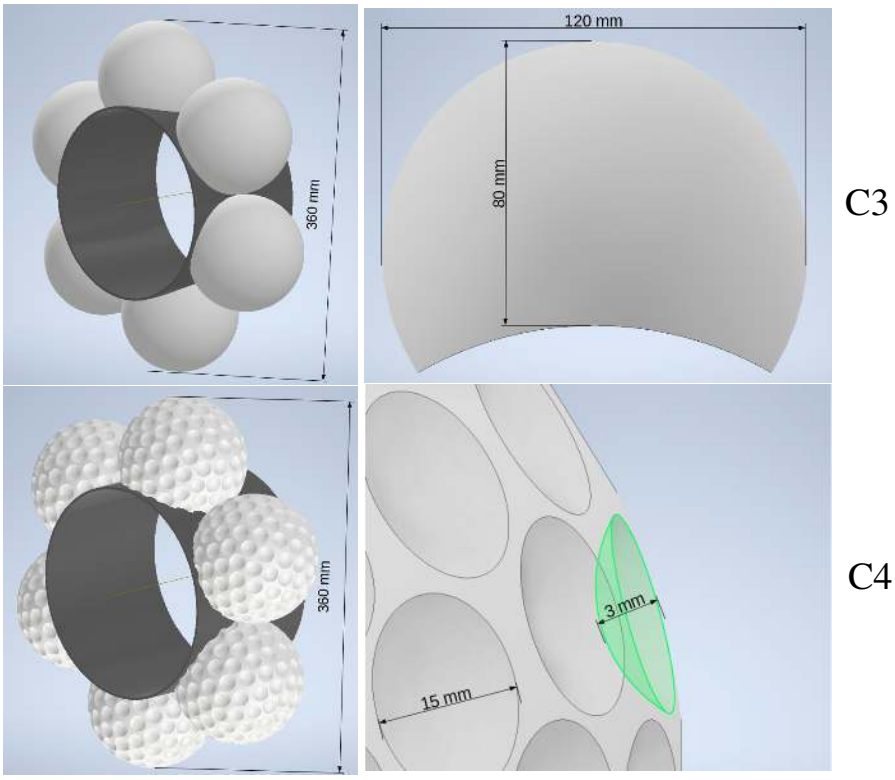

Figure 7: Details of large-scale $C3$ (top) and large-scale with craters $C4$ (bottom) roughness dimensions.

The roughness parameter (e) is defined as the ratio k/D_e, where k is the dimension of the studied roughness and D_e the equivalent diameter, defined in Ameryoun et al. [4]. In the literature, several definitions of the

roughness exist, see Jusoh and Wolfram [10] or Achenbach and Heinecke [1]. k represents the whole marine growth layer, from the surface cable to the extremity of the marine growth. The equivalent diameter is generally defined [10] as being the superimposition of the original diameter of the cylinder (cable or riser) with the close roughness layer. Indeed, a biofouling cover may be composed of a closed layers and an external one. The closed layers below the external one represent a thickness of closed surfaces where no fluid dynamic is permitted, with no entrapped water volume, see Marty et al. [12]. For all studied configurations, the roughness parameter is therefore considered as the external layer where the fluid can pass through the roughness. In the mussel cases, the equivalent diameter (D_e) is calculated as $D_e = D_i + 2 \times (th - k)$ in order to respect the definition previously explained. For the coral cases the cover switches directly from a closed layer corresponding to the internal diameter (D_i) to an opened one (D_{ext}) as represented in Figure 8 and $th = k$. Therefore, in this case, the equivalent diameter is equal to the internal one and $De = Di$.

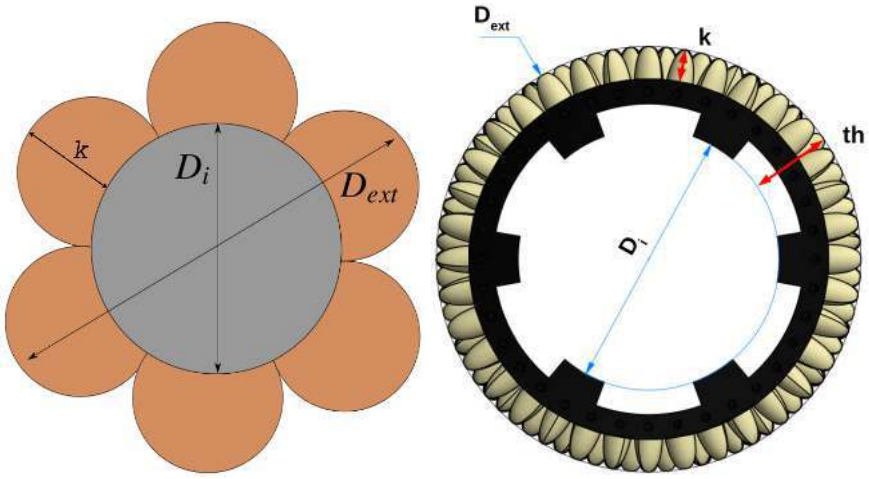

Figure 8: Definition of roughness parameters adapted to the experimental set-up for corals (left) and for mussels (right).

The table 1 provides the characteristics of the configurations tested in the present work with $D_e \in [160; 220]$ and $e \in [0; 0.4]$. In this study, the cylinder is fully covered by a relative roughness for C1 to C4 and partially for C1/S and C2/S. As an essential parameter, the areal densities are also given in table 1 with specimens/m² between 57 (for corals) and 2969 (for mussels). The global blockage ratio (B) and the vertical one (B_v) are also given to help following analyze results and discussion.

Tests have been carried out in current only first, then in oscillating movements without current and finally, the combination of both. The table 2 summarizes the main test conditions which have been imposed to all cases (S, $C1$ to $C4$). In this table, U is the current speed, A_x the motion amplitude (along x) and f the frequency of the hexapod.

All the results are presented as a function of the classical normalized numbers which are defined as follows:

- Reynolds number (R_e) defined in two different ways depending on the choice of the reference speed, the flow velocity U or the oscillation speed $A_x\,\omega$:

$$R_e = \frac{UD_e}{\nu} \quad \text{or} \quad Re = \frac{A_x\,\omega D_e}{\nu}, \text{ with } \nu \text{ the kinematic viscosity.}$$

	S	C1	C2	C1/S	C2/S	C1/C2	C2/C1	C3	C4
$D_i\ (mm)$	160	160	160	160	160	160	160	200	200
$D_{ext}\ (mm)$	160	260	280	220	232	268	272	360	360
$B = (D_{ext}/(w_t * h_t))$	4%	6%	7%	5%	6%	7%	7%	9%	9%
$B_v = (D_{ext}/h_t)$	8%	13%	14%	11%	11%	13%	13%	18%	18%
$k\ (mm)$	0	20	30	12	18	24	26	80	80
$th\ (mm)$	0	50	60	30	36	54	56	80	80
$D_e\ (mm)$	160	220	220	196	196	220	220	200	200
$e = k/D_e$	0	0.091	0.136	0.061	0.092	0.11	0.12	0.4	0.4
$Mass\ (kg)$	47	105	110	85	93.5	107	108	167	167
$Areal\ Density\ (S\ pecimen\ Nb/m^2)$	-	2969	1374	1781	825	2331	2012	57	57

Table 1: Synthesis of the studied roughness parameters for all the studied configurations: current, motion, current+motion (see Table 2).

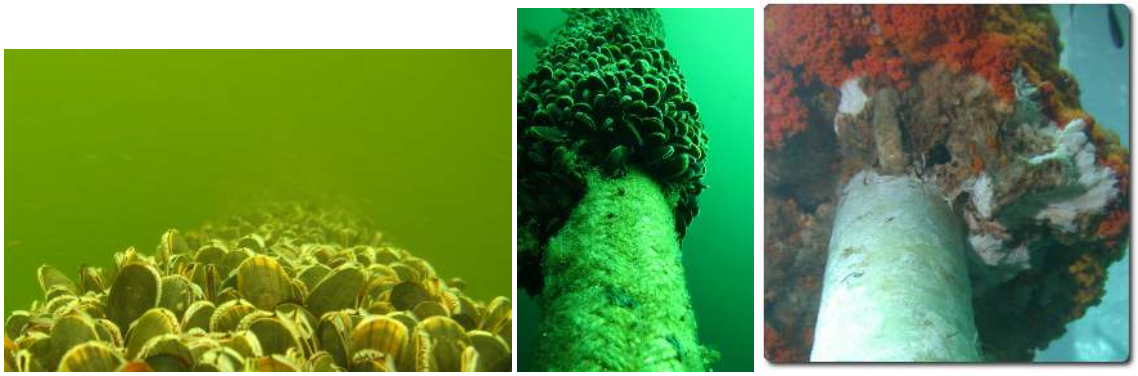

Figure 9: Illustration of mussels and corals colonisation on a 100 mm diameter moorin line (left and center) and on a 200 mm diameter jacket leg (right) [15].

	Current Alone	Motion Alone	Current + Motion
U $(m.s^{-1})$	0.25 - 1.5	-	0.25 - 1.5
Amplitude $A_x\ (mm)$	-	100 - 400	100 - 400
Frequency $f\ (Hz)$	-	0.1 - 0.75	0.1 - 0.75

Table 2: Flow and motion parameters for the tested configurations with A_x and f the motion amplitude and frequency, used for all the tested cases: S ; $C1$ to $C4$; $C1/S$; $C2/S$ and $C1/C2$ (see Table 1).

- Keulegan-Carpenter number (KC) defined by the equation :

$$KC = 2\pi \frac{A_x}{D_e} \tag{1}$$

- The reduced speed (U_r) for current and movements cases :

$$U_r = \frac{U}{fD_e} \quad \text{with} \quad f = \frac{\omega}{2\pi} \tag{2}$$

As well known, it is challenging to find a correlation between the hydrodynamic coefficients (drag, lift, inertia, added mass coefficients) and the many dimensionless numbers (Re, KC, Ur, Stokes...), as the coefficients attempt

to capture multiple hydrodynamic phenomena, each acting with its own amplitude, frequency and phase. In this study, we attempt to better estimate these coefficients in presence of macro-roughness by using usual definition of dimensionless number. Table 3 summarizes the value ranges of the three normalized numbers used in this study, illustrating the wide range of hydrodynamic conditions covered.

Configuration	S	C1-C2-C1/C2-C2/C1	C1/S-C2/S	C3-C4
KC	3.9 - 15.7	2.5 - 11.4	2.8 - 12.5	1.7 - 7.0
U_r	4.1 - 39.1	3 - 56.8	3.2 - 58	1.8 - 17.4
$Re/10^5$	0.4 - 2.7	0.55 - 3.8	0.5 - 3.3	0.9 - 6.1

Table 3: Synthesis of the normalized numbers covered for all configurations.

2.3. Calculation of hydrodynamic coefficients

This section presents the method used to calculate the hydrodynamic coefficients based on the Morison's decomposition (Morison et al. [14]). The recording time is fixed to 256 secondes for all tests in order to ensure convergence of the calculated load averages. The recording frequency is fixed to 128 Hz for the loads cells and 100 Hz for the movements of the hexapod. The synchronisation between the hexapod and the loads cells allows to calculate the phase shifting between the forces on the structure and the movements.

In current only, the drag coefficient is calculated as follow:

$$C_D = \frac{2 \times \overline{F_D(t)}}{\rho S U^2} \tag{3}$$

with ρ the density of water ($\rho = 998\ kg/m^3$), $S = D_e \times L$ the cylinder section in front of the flow and U the current velocity. $\overline{F_D(t)}$ is the temporal mean of the drag $F_D(t)$. This coefficient is also called the *steady-flow drag coefficient*.

In the case of oscillating motions, the hexapod moves along the Ox axis, collinear with the current. The hexapod movements are oscillating with an amplitude A_x and a pulse $\omega = 2\pi f$ such as: $x(t) = A_x \cos(\omega t + \varphi_x)$. It is assumed that the answer of this excitation is a sinusoidal function as well (harmonics higher than 1 are neglected). Thus, the drag effort may be expressed as follows.

$$F_D(t) = F_m \cos(\omega t + \varphi_F) \tag{4}$$

Hence, with $\varphi = \varphi_F - \varphi_x$ it comes :

$$F_D(t) = F_m \cos(\omega t + \varphi_F + \varphi_x - \varphi_x) = F_m \cos(\omega t + \varphi_x) \cos(\varphi_F - \varphi_x) - F_m \sin(\omega t + \varphi_x) \sin(\varphi_F - \varphi_x) \tag{5}$$

$$F_D(t) = -\frac{F_m \cos(\varphi)}{A_x\, \omega^2}\ \ddot{x}(t) + \frac{F_m \sin(\varphi)}{A_x\, \omega}\ \dot{x}(t) \tag{6}$$

Equation 6 can be compared with the Morison's equation [14] :

$$F_D(t) = -\rho C_m L \frac{\pi {D_e}^2}{4}\ \ddot{x}(t) + \frac{1}{2}\rho C_d D_e L\ \dot{x}(t)\ |\dot{x}(t)| \tag{7}$$

with C_m the inertia coefficient ($C_m = C_a + 1$), with C_a the added mass coefficient and C_d the drag coefficient. Moreover, $\sin \omega t\ |\sin \omega t|$ can be approximated with :

$$\sin \omega t\ |\sin \omega t| \simeq \frac{8}{3\pi} \sin \omega t \tag{8}$$

And finally, by comparison:

$$\begin{cases} C_m = \dfrac{F_m \cos(\varphi)}{\rho L \frac{\pi D_e^2}{4} A_x \, \omega^2} \\ \\ C_d = \dfrac{F_m \sin(\varphi)}{\frac{4}{3\pi} \rho D_e L A_x^2 \, \omega^2} \end{cases} \tag{9}$$

For current and motion cases it is assumed that the drag effort can be divided into two parts, the mean drag part $\overline{F_D(t)}$ and the oscillating part $F_m \cos(\omega t + \varphi_F)$, such as:

$$F_D(t) = \overline{F_D(t)} + F_m \cos(\omega t + \varphi_F) \tag{10}$$

Thus, the three coefficients C_D, C_m ans C_d can be calculated similarly as above (equations 3 and 9). It can be noted that these coefficients are the same as those presented in Verley [27]. In the following, these parameters are plotted as a function of the dimensionless numbers previously cited (R_e, KC and U_r).

The accuracy of Morison's method to calculate hydrodynamic coefficients has been discussed in Marty et al. [11] where it is concluded that the method reaches certain limits but is overall a good force predictor for specific applications like the one presented in this paper.

3. Roughness effect on cylinder loads

In this section, we present the experimental results of the tested configurations (S, $C1$, $C2$, $C1/S$, $C2/S$, $C1/C2$, $C2/C1$, $C3$, $C4$) under current conditions first, then oscillating motions only and finally the combination of both loads. For current trials, the drag force and the mean drag coefficient are an alysed. By means of the Morison method, added mass and inertia coefficients are then investigated for oscillating tests and oscillating motions plus current tests.

3.1. Effects of roughness under current conditions

Figure 10 shows the evolution of the drag forces according to the flow v elocity. The curves highlight the classical evolution according to a square power law for the rough cylinders. The rough configurations ($C1$, $C2$, $C1/C2$, $C2/C1$) do not show significant drag force d ifferences. The two partially rough configurations ($C1/S$ and $C2/S$) follow the same pattern as the rough ones but slightly below, about 25% lower. These results show a difference with the two large-scale roughness configurations ($C3$ and $C4$) especially from $U = 1\ m/s$ where the $C4$ drag force is about 15% higher than the $C3$ even if the difference in diameter is less than 4 %. The response is however different for the smooth cylinders (S) with a classical evolution until the transition obtained at a flow speed of 1 m/s. For $U > 1\ m.s^{-1}$, the drag is quite constant around $F_D \approx 200N$.

Figure 11 presents the evolution of the mean drag coefficient (C_D) as a function of the Reynolds number (R_e). As explained in Marty et al. [11], for the smooth case, the overall shape of the $C_D(Re)$ curve clearly coincides with the results presented in the literature, see Schlichting [19]. In the subcritical Reynolds number regime a nearly constant value for C_D of about 0.9 is found. If we correct the theoretical drag coefficient ($C_D = 1.2$) with the reduction factor recommended by standards for finite length member and corresponding to the ratio used in this campaign ($L/D = 12.5$ for smooth case) which is equal to 0.7, we find approximately the calculated mean drag coefficients of this study ($1.2 \times 0.7 = 0.84$). Moreover, this three-dimensional aspect highlights that in this

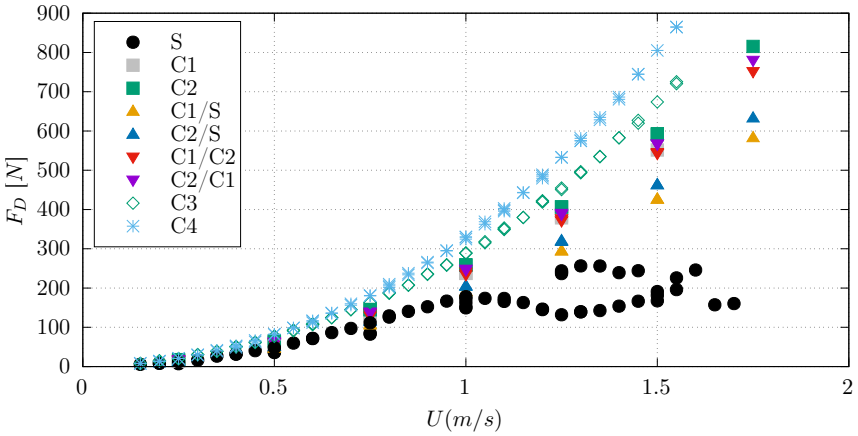

Figure 10: Drag force evolution for the seven tested cases as function of the flow speed U.

work, inertia related phenomena and calculated drag coefficients are always slightly underestimated compared to an infinite cylinder where the three-dimensional aspect is negligible. In the other hand, Szepessy and Bearman Szepessy and Bearman [22] show that at some Reynolds numbers (10^4 - 10^5), the use of appropriate end plates can give a more two-dimensional flow, which then results in an increase in both the fluctuating lift and mean drag. This phenomenon can explain the reason why the drag coefficient shown on our paper is in the lower part of the bibliographical results (i.e. close to 1). The curve highlights a critical transition of the flow behavior around $R_e = 2.2 \times 10^5$ but only for the smooth cylinder case. This results is confirmed by Subrata [21] who shown that increased roughness moves the drag crisis transition area to lower values of Reynolds numbers and is much less pronounced. As confirmed by Allen and Henning [2], with sufficient roughness, the drag crisis can even be eliminated. As in the drag forces graph, the values of C_D for both large-scale roughness ($C3$ and $C4$) are significantly higher (around 50%) and the values of the $C4$ configuration (with small craters in addition of the large-scale roughness) are clearly higher in this graph (15% higher for $R_e/10^5 = 3$). The presence of micro roughness superimposed to a large macro roughness has an important impact on the evolution of the drag phenomena, especially for Reynolds number higher than $R_e = 1.5 \times 10^5$.

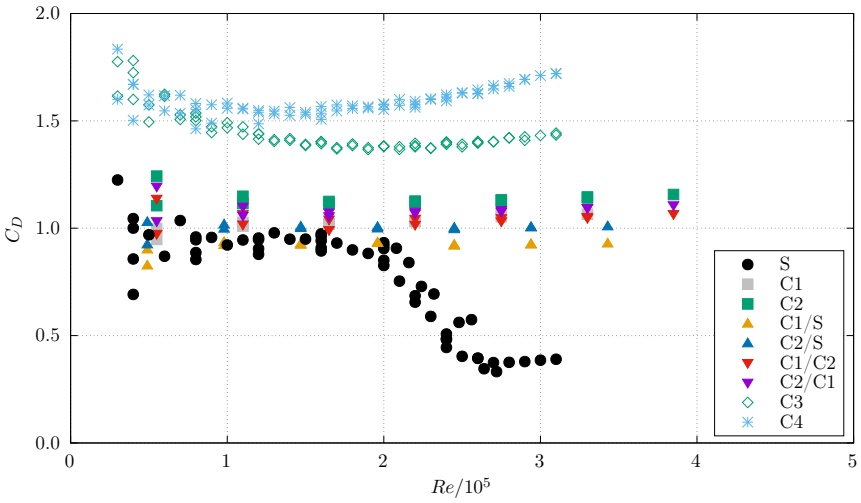

Figure 11: Distribution of C_D as function of the Reynolds number from direct force measurements for all the tested cases.

The results show that the presence of a large-scale roughness leads to significantly increase the drag coefficient (about 50%) compared with smaller roughness such as mussels. Moreover, the behavior of the mean drag coefficient for low Reynolds number ($R_e/10^5 < 1$) does not highlight any difference between the two large-scale cylinders ($C3$ and $C4$), whereas for higher R_e the large-scale configuration with added micro roughness can lead to an increase of 15% compared with the one without micro roughness.

The roughness influence on the lift coefficient has been studied in Marty et al. [11] for the mussel cases and leads to the following conclusions: the presence of roughness allows to reduce physical phenomena related to vortex shedding with the appearance of low frequency components and a reduction of the main peak frequency in the spectral domain. The roughness lead to homogenize the turbulent flow around the cylinder and reduce vortex induced vibrations phenomena. The same behavior is observed for the coral configurations. Thus, for all the studied rough cases, the lift fluctuations are very low with r.m.s. values << 0.05.

3.2. Effects of roughness under wave conditions

Trials presented in this section have all been obtained without current, only with horizontal imposed oscillating motions. Figure 12 presents the evolution of the oscillating drag coefficient (C_d) as a function of the Keulegan-Carpenter number (KC). As previously, these results highlight a significant difference between the mussel cases ($C1$, $C2$, $C1/S$, $C2/S$, $C1/C2$, $C2/C1$) and the coral cases ($C3$ and $C4$) especially for $KC < 8$ where large-scale coefficients can be 4 times higher. In this case, the flow dynamic around the bulbous shape governs the load variations. The oscillating drag coefficient of the mussel cases is 2 times higher, over the entire KC range, than for the smooth cylinder.

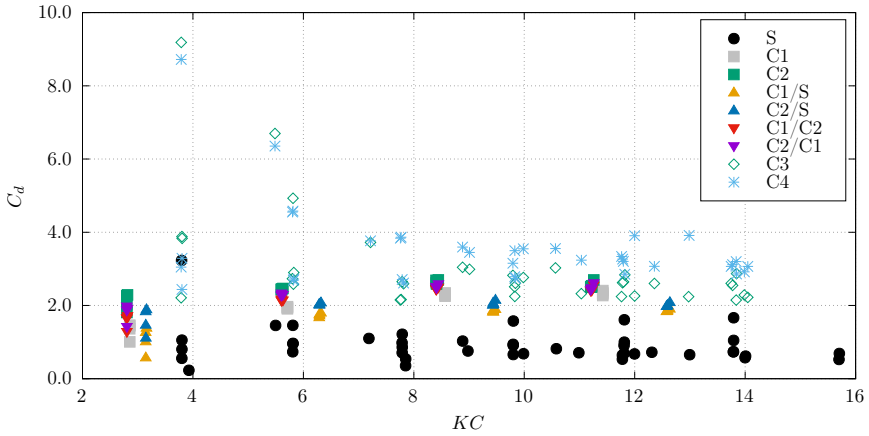

Figure 12: Oscillating drag coefficient for the studied configurations as function of the Keulegan-Carpenter number KC.

The same conclusions can be drawn for the inertia coefficients presented in Figure 13 as a function of K_C. The behavior of the large-scale coefficients ($C3$ and $C4$) are strictly identical but higher compared with the mussels cases ($C1$, $C2$, $C1/S$, $C2/S$, $C1/C2$, $C2/C1$) which were globally equals.

As for the previous test conditions, the inertia coefficients and the oscillating drag coefficients increase with the roughness, but not in a linear tendency with the roughness parameter e. Nevertheless, the coefficients values of the large-scale roughness are significantly higher than those obtained with mussels configurations. And these differences seem even more important when the KC number is low, even if these values are obtained for slight

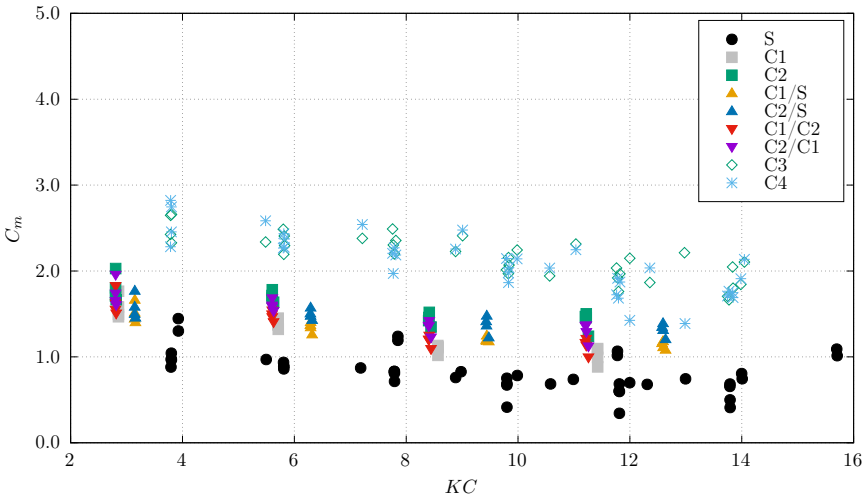

Figure 13: Inertia coefficient for the studied configurations as function of the Keulegan-Carpenter number KC.

sea states thus with low lift force values. In figure 12, it is obvious that the behavior of the oscillating drag coefficient for $C3$ and $C4$ configurations follows two different regimes. A first one for $KC < 7$ where the coefficients are very high then rapidly decrease to reach a second phase where the coefficients evolve constantly with the Keulegan-Carpenter number. These results highlight two issues, the non linear behavior of Cd and C_m according to the relative roughness e and the large scatter in the estimation of the hydrodynamic coefficients for the large roughness especially for low KC (weak amplitudes of motions). This changing regime may be attributed to a global flow driven by fluctuations of local ball wake below $KC = 6$ and by the global turbulent wake of the entire cylinder above. A PIV analysis may help to identify this changing regime. This conclusion is of first importance for structural reliability assessment Ameryoun et al. [4].

3.3. Effects of roughness under wave and current conditions

This section presents results concerning current and oscillating motions test cases. The same coefficients previously shown for the two other test conditions are calculated: i.e. the mean drag coefficient C_D (see Figure 14), the oscillating drag coefficient C_d (see Figure 15) and the inertia coefficient C_m (see Figure 16). These coefficients are presented as a function of the reduced speed (U_r). It was shown in Marty et al. [11] that the behavior of the two drag coefficients (C_D and C_d) for mussels configurations were highly dependant on the amplitude of the oscillating motions for a fixed frequency. The evolution of these coefficient were however quite similar for each rough configuration. Comparing these results with the coral configurations $C3$ and $C4$, it is shown that in the studied range of the reduced speed, the behavior of the large-scale coefficients fits very well with the mussels results ($C1$, $C2$, $C1/S$, $C2/S$, $C1/C2$, $C2/C1$). The $C4$ configuration (large-scale + micro roughness) leads to the largest mean coefficient and is significantly higher compared with $C3$ and other rough configurations. This figure clearly shows that for high values of U_r all curves converge to $C_D = 1$

Figure 15 presents the evolution of the oscillating drag coefficient C_d and shows an opposite behavior from the averaged drag coefficients C_D: value of the coefficient C_d increases with the reduced velocity U_r. Moreover, for a fixed frequency (or fixed U_r) the amplitude parameter has a big impact and the value of the coefficient increases when the amplitude A_m decreases. This figure does not highlight any difference between all the rough

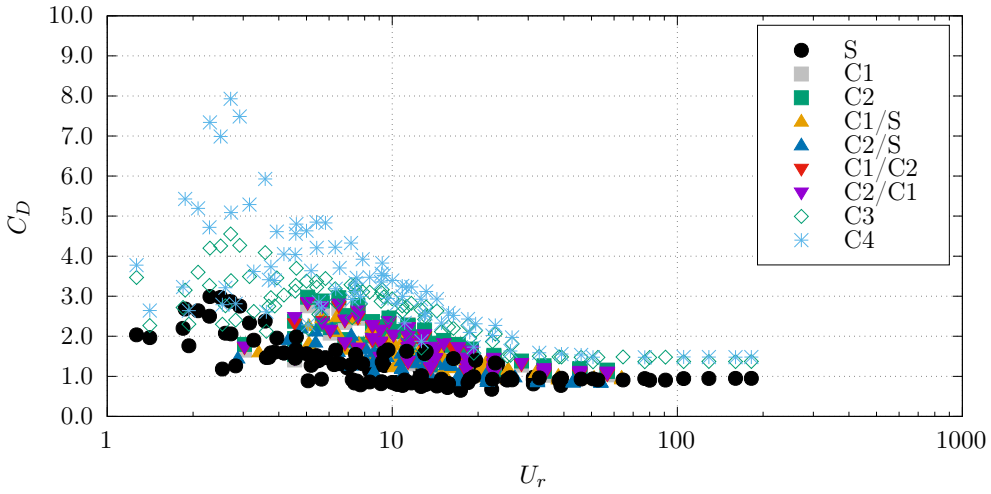

Figure 14: Mean drag coefficient C_D as function of the reduce speed U_r for the tested configurations.

configurations, corals or mussels, but only a difference with the smooth cylinder for which coefficients evolve the same way but with significantly lower values (about 20% lower).

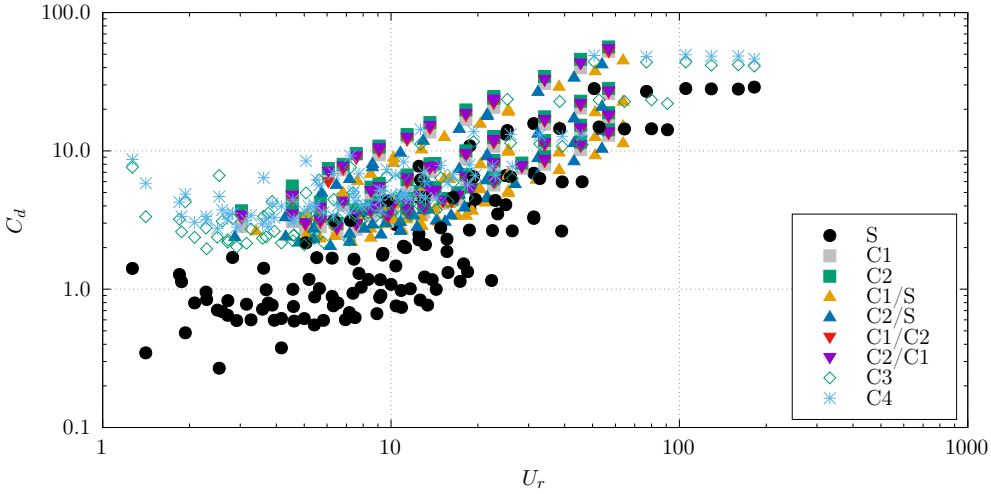

Figure 15: Oscillating drag coefficient C_d as function of the reduce speed U_r for the tested configurations.

It has been demonstrated in [11] that the behavior of the inertia coefficient (C_m) is similar for each mussel configuration independently of the oscillating motions or the oscillating frequency. It seems to be still the case for large-scale configurations ($C3$ and $C4$). Indeed, all curves fit quite well in the reduced speed range between 5 and 80 ($5 < U_r < 80$).

The comparison between smooth, mussel or coral roughness under wave and current excitation shows that we have common behavior between a realistic marine growth (around $k/D = 0.1$) and a large-scale marine growth with very large roughness ($k/D = 0.4$) as it is the case here. For the two other test cases (current only and motions only) the results show significant differences between the two kinds of roughness, but these differences seem to decrease for combined current and motion loading.

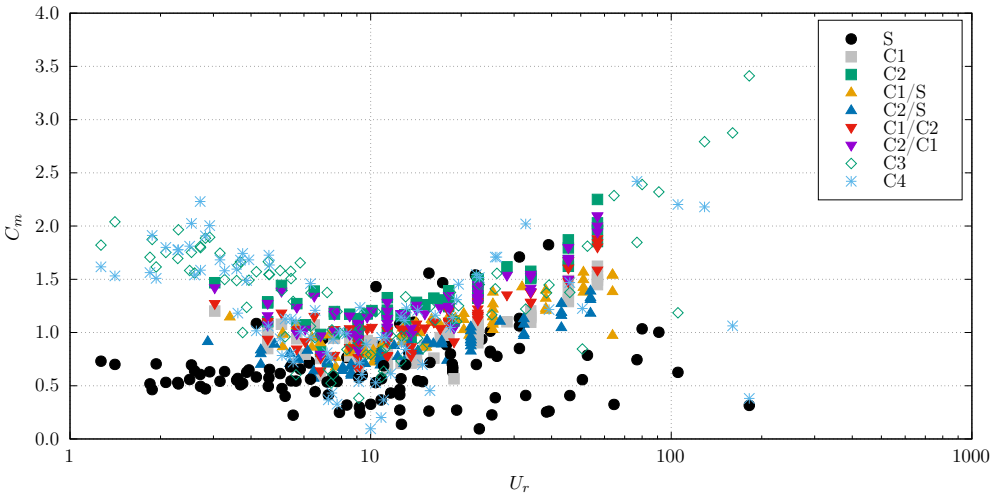

Figure 16: Inertia coefficient C_m as function of the reduce speed U_r for the tested configurations.

4. Discussion

This work provides a comparison study between eight hard macro-roughened configurations placed in similar current and wave conditions. It shows that using an equivalent diameter corresponding to the close volume of the system, results between rough configurations are significantly different according to the size of the roughness. Especially for drag coefficients where results found for large size roughness can be up to four times higher than those obtained with a smooth cylinder and two times higher for large-scale roughness ($k/D_e = 0.4$) compared with smaller roughness ($k/D_e = 0.14$). This method has the advantage to highlight the impact of the roughness on the hydrodynamic behavior of the studied system.

In order to highlight the influence of the equivalent diameter definition, the previous coefficients have been calculated using a different equivalent diameter. The coefficients are then calculated using two specific equivalent diameters. One for the drag coefficients (C_D and C_d), based on the projected area of the system (called D_S) and another one for the inertia coefficients (C_m), based on the total volume of the system (called D_V). The first one is calculated dividing the projected surface S_P in the plane normal to the flow (including the roughness) by the length of the cylinder L, given by the equation (11). The second one is calculated using the total volume V of the system (cylinder + roughness) as shown in the equation (12). D_S is then introduced in the equations (3) and (9) for the calculation of the mean drag and oscillating drag coefficients. D_V is injected in the equation (9) for the calculation of the inertia coefficient.

$$D_S = S_p/L \tag{11}$$

$$D_V = \sqrt{\frac{4 \times V}{\pi \times L}} \tag{12}$$

The table 4 provides the equivalent diameters (D_S, D_V and D_e) for each studied configuration.

Figure 17 represents a comparison between the drag coefficient C_D calculated from both equivalent diameter, D_e on the left and D_S on the right. The use of D_S clearly fits all the curves around 1 highlighting that as soon as

Configurations	S	C1	C2	C1/S	C2/S	C1/C2	C2/C1	C3	C4
D_S (mm)	160	250	260	214	220	254	256	326	326
D_V (mm)	160	235	241	205	209	237	239	302	302
D_e (mm)	160	220	220	196	196	220	220	200	200

Table 4: Synthesis of the studied roughness parameters for all configurations.

the surface is rough enough, the same mean drag coefficient can be used for drag estimation with the equivalent surface diameter.

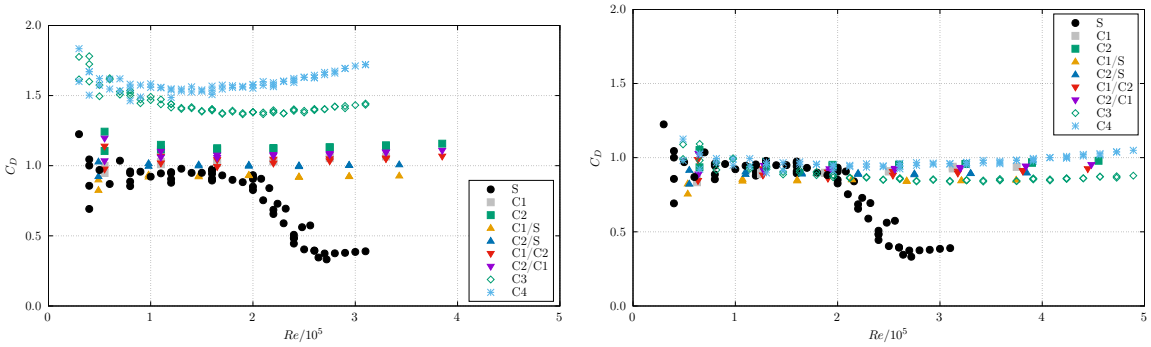

Figure 17: Distribution of C_D as function of the Reynolds number from direct force measurements for all the tested cases. Calculated with D_e on the left and with D_S on the right.

Figure 18 and 19 represent respectively the oscillating drag coefficient C_d and the inertia coefficient C_m for trials under motions excitation only, for both equivalent diameters. Calculated with D_e on the left and with D_S or D_V on the right. As for the previous case, the use of D_S and D_V for the calculation of C_d and C_m tends to flatten all the curves into a single one. Especially for the inertia coefficient where all curves fit around $C_m = 1$. The comparison of the drag coefficient on Figure 18 still shows certain differences between the two kinds of rough configurations for $KC < 4$. Nevertheless, the use of the projected surface diameter leads to a common behavior of the coefficients for all the rough cases.

Figure 20, 21 and 22 represent respectively the inertia coefficient C_m, the oscillating drag coefficient C_d and the mean drag coefficient C_D for wave and current excitation, calculated with D_e on the left and with D_S or D_V on the right.

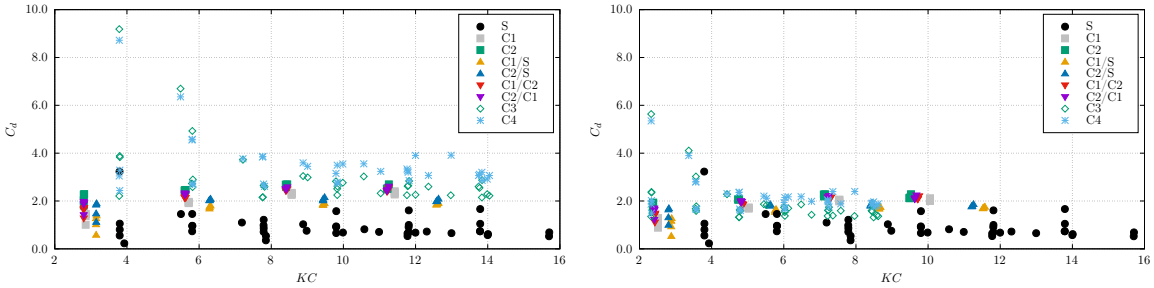

Figure 18: Oscillating drag coefficient for the studied configurations as function of the Keulegan-Carpenter number KC. Calculated with D_e on the left and with D_S on the right.

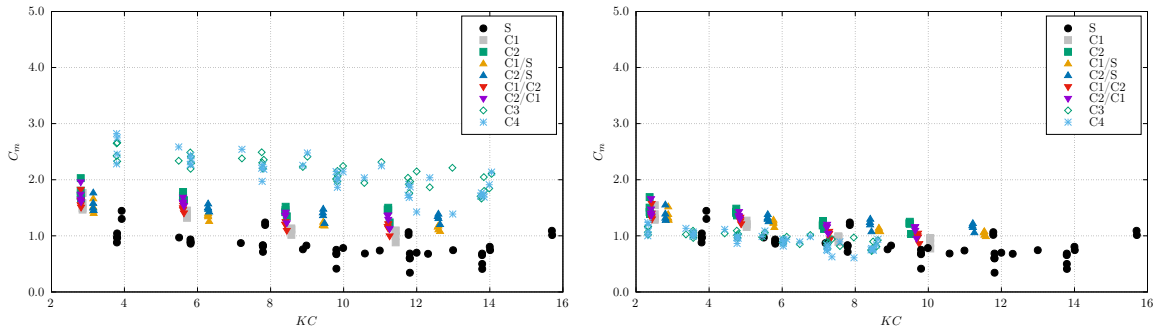

Figure 19: Inertia coefficient for the studied configurations as function of the Keulegan-Carpenter number KC. Calculated with D_e on the left and with D_V on the right.

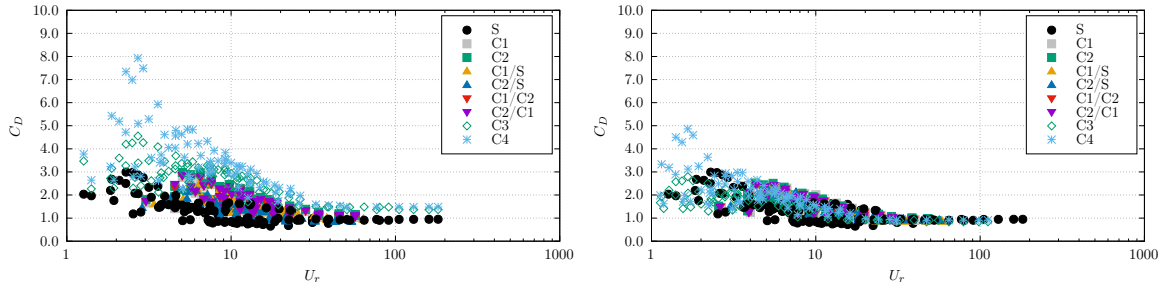

Figure 20: Mean drag coefficient C_D as function of the reduce speed U_r for the tested configurations. Calculated with D_e on the left and with D_S on the right.

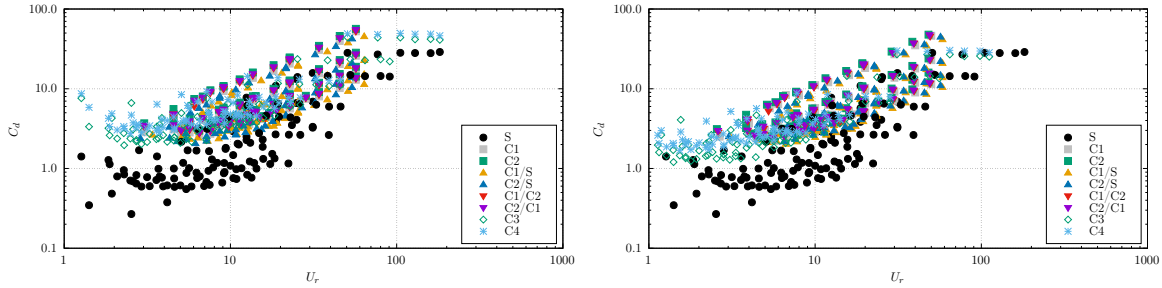

Figure 21: Oscillating drag coefficient C_d as function of the reduce speed U_r for the tested configurations. Calculated with D_e on the left and with D_S on the right.

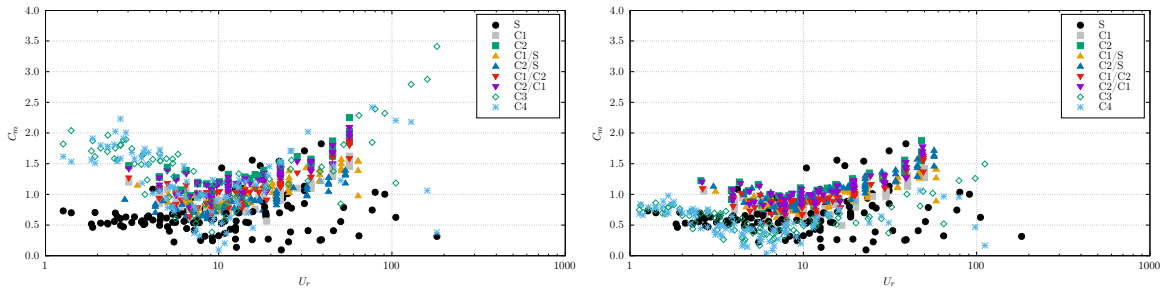

Figure 22: Inertia coefficient C_m as function of the reduce speed U_r for the tested configurations. Calculated with D_e on the left and with D_V on the right.

As obtained in the previous case, the use of a volume diameter for the inertia coefficients and a surface diameter for the drag coefficient leads to flatten all the results especially for the C_D and C_m. We still have some

differences between the rough cases and the smooth ones for the oscillating drag coefficient.
These results highlight that the use of a specific surface or volume diameter leads to flatten the curves and standardize all the results, whatever the size of the roughness, smooth or with large scale roughness such as corals or hard marine growth like mussels. These results prove that the knowledge of the volume and the projected surface of the cylindrical structure (rough or not) could simplify the estimation of the forces that apply on the system. In doing this two important points should be kept in mind:

- The hypothesis of axi-symetrical slender element inherent to Morison formulation supposes a 2D flow. This hypothesis is probably not still valid for macro-roughness so generating turbulent flow of highly 3D nature for which a linear definition of the reference length (diameter and thickness per meter) is not still relevant. In using a projected area similarly to a lifting profile, the reference length becomes a reference surface, so traducing the 2D nature of the obstacle and therefore the 3D nature of the impacted flow. Even if the global blockage ratio is low ($< 10\%$), the vertical one ($Bv = Dext/(wt * ht)$) is between 8 and 18%. These values are high even if only horizontal motion are imposed to the system. Some surface effects (free surface and bottom floor) can influence the results.

- In using the projected area and real volume, the coefficients of $C3$ and $C4$ are in the vicinity of the coefficients found for mussel cases or lower whereas they are significantly higher using the first diameter hypothesis. This effect is directly attributed to the porosity rate of the real volume of protuberance versus the filled annular volume assumed using a single diameter value as reference length. As per shown in the table 3 the use of projected and volume diameters increases with respect to external diameter of respectively 1.15 and 1.0 for $C1$ and $C2$ when this increase is of 1.63 and 1.50 for $C3$ and $C4$. This indicates a porosity rate significantly higher for coral cases, so making the use of external diameter not representative of the colonized volume.

Indeed, whatever the size of the roughness, the knowledge of the drag and the inertia coefficients corresponding to the equivalent smooth system in volume and surface can be sufficient to estimate the overall loads applied on the system. In practice, it seems complicated for on-site measurements to know the volume and the surface projected of the structure on which the hydrodynamics coefficients want to be known. It therefore appears that for direct engineering applications, the measurement of the height of the roughness (k) in order to estimate hydrodynamic coefficients stay the simplest solution.

5. Conclusion

The aim of this work was to compare the hydrodynamic behavior of two large-size macro-roughened cylinder with a high roughness parameter ($0.06 < k/D_e < 0.4$) and representative of hard and large marine growth such as corals or mussels. The results obtained under current conditions, oscillating motions conditions then the addition of both conditions are compared with results obtained with a smooth cylinder under similar tests conditions. Therefore, this work constitute a large database of nine different hard and large-size roughness placed in the same hydrodynamic conditions.
Hydrodynamic coefficient results (drag and inertia) are presented as a function of dimensionless numbers such

as the Reynolds number (R_e), the Keulegan-Carpenter number (KC) and the reduced speed (U_r). All these parameters are calculated from an equivalent diameter D_e defined first as being the superimposition of the original diameter of the cylinder (cable or riser) with the close roughness layer. In this way, for all the tests carried out in this work, the presence of a realistic roughness shows a significant influence on the hydrodynamic behavior of a cylinder subjected to current and wave conditions.

For trials carried out with current only, the presence of a large-scale roughness (corals) leads to significantly increase the drag coefficient (about 50% using the standard Morison formulation) compared with smaller roughness such as mussels. Moreover, these results show a difference with the two large-scale roughness configurations ($C3$ and $C4$) especially from $R_e/10^5 = 1$ where the $C4$ drag coefficient is about 15% higher than the $C3$ one even if the perturbation in diameter is less than 4%.

This behavior is quite similar for test carried out with motions only, the inertia coefficients and the oscillating drag coefficients seem to increase with the roughness without highlighting any difference within the two kinds of roughness, mussels and corals. Nevertheless, the coefficient values of the large-scale roughness are significantly higher than those obtained with mussel configurations. And theses differences seem even more important when the KC number is low.

For the last studied test conditions, waves and current, these differences decrease. The comparison between a smooth cylinder, mussel or coral roughness shows that we have common behavior between a realistic marine growth (around $k/D = 0.1$) and a large-scale marine growth with very large roughness ($k/D = 0.4$).

In a second time, the same coefficients are calculated using a specific equivalent diameter for drag coefficient, based on the projected area of the system, and a specific one for inertia coefficients, based on the total volume of the system. The use of a specific surface or volume diameter leads to flatten all the curves, whatever the size of the roughness. This leads to the conclusion that the use of these two specific equivalent diameter is a better way to normalized the studied parameters. These results prove that the knowledge of the volume and the projected surface of the cylindrical structure could simplify the estimation of the forces that apply on the system. Indeed, whatever the size of the roughness, the knowledge of the drag and the inertia coefficients corresponding to the equivalent smooth system in volume and surface can be sufficient to estimate the overall loads that apply on the system. The underlying question is now: how to determine this value with sufficient precision, depending on the deployment site, the duration of immersion and the ocean-meteorological conditions?

6. Highlights

- Two kinds of hard marine growth are experimentally studied
- Drag and inertia coefficients are calculated from tests with wave and current excitation
- Classical equivalent diameter to nondimensional studied coefficients shows an increase of drag and inertia phenomena with the roughness
- Specific equivalent diameter based on the projected surface for drag phenomena leads to standardize all results

Research data for this article

Data associated with this article have been published in [8] and [13].

Acknowledgments

This work benefits from funding from France Energies Marines as well as the French National Research Agency under the Investments for the Future program bearing the reference ANR-10-IEED-0006-28. This project was partly financially supported by the European Union (FEDER), the French government, IFREMER and the region Hauts-de-France in the framework of the project CPER 2015-2020 MARCO. Authors thank TOTAL and especially Michel and Laetitia Baudet for their implication in this work.

References

[1] Achenbach, E. and Heinecke, E. (1981). On vortex shedding from smooth and rough cylinders in the range of reynolds numbers 6e3 to 5e6. *Journal of fluid mechanics*, 109:239–251.

[2] Allen, D. and Henning, D. (2001). Surface roughness effects on vortex-induced vibration of cylindrical structures at critical and supercritical reynolds numbers. *OTC Offshore Technology Conference*.

[3] American Petroleum Institute (API) (2000). Planning, Designing and Constructing Fixed Offshore Platforms - Working Stress Design. API Recommended Practice 2A-WSD (RP 2A-WSD) twenty-first edition, American Petroleum Institute (API).

[4] Ameryoun, H., Schoefs, F., Barrillé, L., and Thomas, Y. (2019). Stochastic modeling of forces on Jacket-Type offshore structures colonized by marine growth. *Journal of Marine Science and Engineering*, 7(5):158.

[5] Boukinda, M. L., Schoefs, F., QuiniouRamus, V., Birades, M., and Garretta, R. (2007). Marine growth colonization process in guinea gulf: Data analysis. *Journal of Offshore Mechanics and Arctic Engineering*, 129(2):97–106.

[6] Det Norske Veritas (DNV) (2010). Offshore Standard Position mooring. https://rules.dnvgl.com/docs/pdf/dnv/codes/docs/2010-10/rp-c205.pdf, Det Norske Veritas (DNV).

[7] Gaurier, B., Germain, G., Facq, J. V., and Bacchetti, T. (2018). Wave and current flume tank of ifremer at boulogne-sur-mer. description of the facility and its equipment.

[8] Gaurier Benoit, Germain Gregory, F. J.-V. B. T. B. L. B. M. (2018). Marine growth effects on the hydrodynamical forces of a circular cylinder.

[9] Henry, P., Nedrebo, E., and Myrhaug, D. (2016). Visualisation of the effect of different types of marine growth on cylinders' wake structure in low re steady flows. *Ocean Engineering*, 115:182–188.

[10] Jusoh, I. and Wolfram, J. (1996). Effects of marine growth and hydrodynamic loading on offshore structures. *Jurnal Mekanikal*, 1(1):77–86.

[11] Marty, A., Berhault, C., Damblans, G., Facq, J. V., Gaurier, B., Germain, G., Soulard, T., and Schoefs, F. (2021a). Experimental study of hard marine growth effect on the hydrodynamical behaviour of a submarine cable. *Applied Ocean Research*, 114.

[12] Marty, A., Schoefs, F., Soulard, T., Berhault, C., Damblans, G., Facq, J. V., Gaurier, B., and Germain, G. (2021b). Effect of roughness of mussels on cylinder forces from a realistic shape modelling. *Journal of Marine Science and Engineering*, 9(6).

[13] Marty Antoine, Germain Gregory, F. J.-V. G. B. B. T. (2020). Experimental investigation of the marine growth effect on the hydrodynamical behavior of a submarine cable under current and wave conditions.

[14] Morison, J. R., O'Brien, M. P., Johnson, J. W., and Schaaf, S. A. (1950). The forces exerted by surface waves on piles. *Journal of Petroleum Technology*, 2(5):149–154.

[15] Repecaud, M., Tancray, A., and Plus, M. (2021). Colonisation par les moules des lignes de mouillage textiles de la bouée wavegem. *IFREMER*.

[16] Sarpkaya, T. (1976a). In-line and transverse forces on cylinders in oscillatory flow at high reynolds numbers. *Journal of Ship Research*, 21(4):200–216.

[17] Sarpkaya, T. (1976b). Vortex shedding and resistance in harmonic flow about smooth and rough circular cylinders at high reynolds numbers. Technical report, Naval postgraduate school, Monterey CA.

[18] Sarpkaya, T. (1985). In-line force on a cylinder translating in oscillatory flow. *Applied Ocean Research*, 7(4):188–196.

[19] Schlichting, H. (1979). *Boundary layer theory*. McGraw-Hill book compagy, New York.

[20] Schoefs, F. and Tran, T.-B. (2022). Reliability updating of offshore structures subjected to marine growth. *Energies*, 15(2).

[21] Subrata, C. (2005). pages v–viii.

[22] Szepessy, S. and Bearman, P. W. (1992). Aspect ratio and end plate effects on vortex shedding from a circular cylinder. *Journal of Fluid Mechanics*, 234:191–217.

[23] Teng, C. C. and Nath, J. H. (1989). Hydrodynamic forces on roughened horizontal cylinders. *21st Offshore Technology Conferencen Houston, Texas*.

[24] Theophanatos, A. (1988). *Marine growth and hydrodynamic loading of offshore structures*. PhD thesis, University of Strathclyde, Glasgow (UK).

[25] Theophanatos, A. and Wolfram, J. (1989). Hydrodynamic loading on macro-roughened cylinders of various aspect ratios. *Journal of Offshore Mechanics and Arctic Engineering*, 111(3):214–222.

[26] Vanhinsberg, N. P. (2015). The reynolds number dependency of the steady and unsteady loading on a slightly rough circular cylinder: From subcritical up to high transcritical flow state. *Journal of Fluids and Structures*, 55:526–539.

[27] Verley, R. L. P. (1980). *Oscillations of cylinders in waves and currents*. PhD thesis, Loughborough University of Technology.

[28] Xiaojie, T., Daoxi, L., Yingchun, X., Wei, D., and Dashuai, X. (2019). Experimental study on the hydrodynamic characteristics of cylinder with rough surface. *Journal of Marine Science and Technology*, 25:842–848.

[29] Zeinoddini, M., Bakhtiari, A., Ehteshami, M., and Seif, M. S. (2016). Towards an understanding of the marine fouling effects on viv of circular cylinders : Response of cylinders with regular pyramidal roughness. *Applied Ocean Research*, 59:378–394.